Harris, Christopher and Baptiste, Joshua and Lindgren, Eric B. and Besley, Elena and Stace, Anthony J. (2017) Coulomb fission in multiply charged molecular clusters: experiment and theory. Journal of Chemical Physics, 146 (16). 164302/1-164302/10. ISSN 1089-7690

Coulomb fission in multiply charged molecular clusters: Experiment and theory

Christopher Harris, Joshua Baptiste, Eric B. Lindgren, Elena Besley and Anthony J. Stace*

Department of Physical and Theoretical Chemistry, School of Chemistry, University of Nottingham, University Park, Nottingham NG7 2RD, U.K.

A series of three multiply charged molecular clusters, $(C_6H_6)_n^{z+}$ (benzene), $(CH_3CN)_n^{z+}$ (acetonitrile), and $(C_4H_8O)_n^{z+}$ (tetrahydrofuran), where the charge *z* is either 3 or 4, have been studied for the purpose of identifying patterns of behaviour close to the charge instability limit. Experiments show that on a time scale of ~10^{-4} s, ions close to the limit undergo Coulomb fission where all of the observed pathways exhibit considerable asymmetry in the sizes of the charged fragments, and are associated with kinetic (ejection) energies of between 1.4 and 2.2 eV. Accurate kinetic energies have been determined through a computer simulation of peak profiles recorded in the experiments and the results modelled using a theory formulated to describe how charged particles of dielectric materials interact with one another (Bichoutskaia *et al. J. Chem. Phys*. **2010,** *133*, 024105). The calculated electrostatic interaction energy between separating fragments gives an accurate account for the measured kinetic energies and also supports the conclusion that +4 ions fragment into +3 and +1 products as opposed to the alternative of two +2 fragments. This close match between theory and experiment supports the assumption that a significant fraction of excess charge resides on the surfaces of the fragment ions. It is proposed that the high degree of asymmetry seen in the fragmentation patterns of the multiply charged clusters is due, in part, to limits imposed by the time window during which observations are made.

I. INTRODUCTION

Following the first observation of molecular clusters in a mass spectrometer, the existence and stability of multiply charged collections of molecules has been a subject of considerable interest and speculation.[1-7] To date, those multiply charged molecular clusters that have been the subject of experimental measurement have exhibited a lower size limit, below which they become unstable due to Coulomb repulsion between the resident charges.[1] There have been numerous experimental attempts to observe the process of Coulomb fission that should accompany the instability of molecular clusters,[1,4,5,6,8] and although charge separation has been observed in photoexcited multiply charged clusters of metal atoms,[9] until recently,[10,11] attempts to observe similar processes in size-selected molecular clusters have not been particularly successful. Last, Jortner and coworkers have complemented the experimental work through their predictions of the fission pathways for highly charged atomic and molecular clusters.[12]

Coulomb fission in a cluster can be broken down into two subprocesses: (i) the breakup of a multiply charged cluster into two closely associated charged fragments and (ii) rapid separation of the fragments driven by electrostatic repulsion. If steps (i) and (ii) are not spontaneous, then the implication is that any delay in Coulomb fission is caused by the presence of a potential energy barrier, which impedes separation of the charges and/or the fragments. Figure 1 shows a schematic of the various barriers that could exist when a multiply charged molecular cluster, M_n^{z+}, breaking up into two charged fragments. Detailed calculations of the energy surfaces experienced by dication clusters composed of a range of dielectric materials, showed that the presence or absences of a barrier to the *separation* of two charged fragments depended strongly on the polarizability of the material concerned.[11] If fission results in just two

fragments, then the Coulomb repulsion that accompanies their separation should lead to a significant release of kinetic energy, and estimates from previous experiments range from 0.2 to 1 eV.[1,6,7,13] However, it has been shown earlier that a simple point charge calculation of the kinetic energy release expected for a dication cluster composed of a dielectric material gives a very unrealistic estimate for the location of the two charges.[11]

Apart from earlier studies of triply charged CO_2 and NH_3 clusters,[1,8] neither of which included any size-dependent data, there have been no recorded examples of the delayed Coulomb fission of multiply charged molecular clusters. For doubly charged clusters, the failure to observe Coulomb fission has been attributed to a presence of compression modes,[1,14] which when excited by Coulomb repulsion can dissipate large amounts of energy from a cluster via monomer evaporation. A previous study of the collision-induced fragmentation of triply charged benzene clusters showed that excitation promoted charge separation, which was accompanied by extensive neutral molecule loss .[5]

An estimate of the critical number of molecules required to stabilize a multiply charged cluster can be obtained from the Rayleigh instability relationship: $(ze)^2/n_{cr} = 64\pi^2\gamma\varepsilon_0 r_0^3$, which is based on a classical liquid-drop model,[15] and where ze is the total charge, n_{cr} the critical number of molecules required to stabilize a cluster against the Coulomb repulsion present between two or more charges, γ the surface tension, r_0 the radius of a constituent molecule, and ε_0 the permittivity of free space. For multiply charged clusters much of the discussion centres on n_{cr} and patterns of behaviour identified in individual clusters of size n in terms of the ratio $[n_{cr} / n] = X$, where X is a fissility parameter.[12] From an energetic view point, X can also be defined as $X = E_{Coulomb}/(2.E_{surface})$;[12] thus identifying the balance between repulsive Coulomb forces and cohesive surface forces and the relative contributions they make to the fission barrier. For $X < 1$ fission over a barrier is thought to be promoted through thermal/internal excitation, and the prediction is of a few large fragments with low kinetic energies.[12] In contrast, $X > 1$

corresponds to barrierless Coulomb explosion driven by high levels of charge repulsion to give large numbers of small ionic fragments each with a high kinetic energy.[12] Experiments on multiply charged clusters, have devoted considerable attention to identifying patterns of behaviour that might prevail at or close to n_{cr}.[1,4,5,6,8] However, associated with the magnitude of X has to be a timescale over which an appropriate experiment might distinguish between the two extremes of behaviour. Given the timescales on which many typical mass spectrometers operate (~ 10^{-5} s), fission is the most obvious outcome; however, until recently a definitive identification of such a process in a size-selected cluster had not been forthcoming.[10,11] Attempts to capture events on a much shorter experimental time scale include a novel deflection method adopted by Mähr *et al*.[7] and an imaging experiment by Hoener *et al*.,[16] which has succeeded in distinguishing between Coulomb explosion and fission, and has also generated scattering patterns for each type of event.

As far as speculating on patterns of behaviour is concerned, multiply charged clusters should have features in common with the fragmentation steps that are thought to accompany electrospray ionization (ESI).[17-25] Discussions of the final steps of the ESI process have focused on two mechanisms: a charge residue model (CRM) where highly charged ions, such as proteins, are thought to form as a result of extensive solvent evaporation, during which the ion of interest retains or acquires a significant fraction of the total available charge.[26,27] A second mechanism, the ion evaporation mechanism (IEM), is believed to proceed *via* the ejection of small solvated ions and appears to be more applicable to the appearance of relatively small residual ions.[28,29] It has been suggested that CRM and IEM models commence with a combination of evaporation and Coulomb fission, with any differentiation most likely to appear as they approach a final size.[17,18] Both mechanisms have both been the subject of several reviews.[17,18,21]

Observations on the delayed Coulomb fission of *size-selected* dication clusters have been reported in two earlier publications, where experimental measurements of kinetic energy release were successfully interpreted using two separate dielectric particle models.[10,11] In the work presented here, experimental measurements and the application of theory have been extended to a series of *size-selected* triply and quadruply charged clusters in the form of $(C_6H_6)_n^{z+}$, $(CH_3CN)_n^{z+}$ and $(C_4H_8O)_n^{z+}$, where the charge z is either 3 or 4 and where, in each case, n is close in value to the charge instability limit. For each precursor ion, the experiments have recorded two significant pieces of information: (i) the size of each dominant fragment ion; and (ii) the kinetic energy release associated with each fragmentation process. Figure 1 illustrates exactly how these measurements are related to the break-up of a charged molecular cluster of the form M_n^{z+}. Starting from a maximum on the potential energy curve, decay is assumed to involve the separation of two charged spheres with sizes that are determined by the experimental measurements. As they separate, the fragment spheres experience Coulomb repulsion, which finally leads to a release of kinetic energy that is also recorded in the experiment and has a theoretical maximum value given by U_{max}. To interpret the results, reaction potential energy surfaces have been modelled by representing the fission products as charged *dielectric* spheres. These calculations have been undertaken using an analytical solution developed to solve the long-standing problem of how charged spheres of dielectric materials interact with one another.[30] The calculations demonstrate how the electrostatic potential energy between two charged particles depends on the relative dielectric permittivity's, ε_r of the clusters and, for a fixed charge, the ratio of their sizes. For many of the measurements presented here there is excellent agreement between experiment and theory. It is recognized that ε_r is a property that is usually associated with bulk materials, and that it may not be directly applicable to a discussion of charge shielding in finite-sized objects. Therefore, ε_r takes the

form of a parameter, which in the absence of additional information, is given a value for a liquid sample of the corresponding bulk material at 25° C.

II EXPERIMENTAL SECTION

Observations on the fragmentation patterns of multiply charged molecular clusters have been made on an apparatus that combines a high resolution reversed geometry mass spectrometer (VG Analytical ZAB-E) with a pulsed supersonic cluster source. Since details of the experimental procedure have been given previously,[11] what follows is a brief summery. Molecular clusters from each of the liquids were generated by passing argon through the liquid contained in a reservoir cooled in an ice bath. The resultant neutral clusters were ionized by 70 eV electrons and the ion beam extracted from the ion source at a potential of +7 kV into the flight tube of the mass spectrometer. Cluster ions with a particular combination of charge (z_1) and mass (m_1) were selected using a magnet and the ionic products of Coulomb fission in the field free region between the magnet and an electrostatic analyser (ESA) were identified by scanning the voltage on the latter. The field-free region is 1.5 m in length and ions are approx. $5x10^{-5}$ s old when they enter that section of the mass spectrometer. This link-scanning procedure provides a mass-analysed ion kinetic energy (MIKE) spectrum,[31] which can be used to identify ionic fragments according to their laboratory-frame kinetic energy and the energy spread in a peak can be related to the centre-of-mass kinetic energy released during fragmentation.[31] To detect the principal charged products from the fission of a multiply charged cluster, the ESA was scanned to record ionic fragments with laboratory-frame kinetic energies from 10 keV downwards. For laboratory-frame kinetic energies of between 7 keV and 10 keV there are no background ion signals from other processes, such as the loss of neutral molecules, which means the very weak signals that arise from Coulomb fission can be recorded without interference. However, this approach does mean that only the largest of the charged fragments

is detected. The size of the smaller fragment is determined from mass and charge balance, together with the assumption that it emerges as a single unit, which is supported by the shapes of peak profiles recorded for Coulomb fission. Attempts to record the smaller of the two fragments were hampered by two factors: (i) the severe instrumental discrimination light ions with high kinetic energies can experience; and (ii) an overlap with peaks arising from the loss of neutral molecules, which has previously been shown to accompany Coulomb fission.[11]

From the magnitude of the electric sector voltage necessary to transmit them, the mass-to-charge ratio of fragment ions can be identified from the following equation:[31]

$$E^* = \frac{m_2}{m_1}\frac{z_1}{z_2} E_0 \qquad (1)$$

E_0 is the initial parent ion kinetic energy (7 keV), E^* is the kinetic energy after fragmentation and m_2 and z_2 are the mass and charge, respectively, of the fragment ion being detected. Ions were detected with a Daly scintillation detector linked to a lock-in amplified (Stanford Research Systems SR850), which provided phase-sensitive detection referenced with respect to a train of nozzle pulses. During the course of these experiments, the background pressure beyond the ion source remained less then $1x10^{-7}$ mbar, thus ensuring minimal interference from collision induced fragmentation.

Figure 2 shows an example of a MIKE scan recorded from the triply charged cluster ion $(C_6H_6)_{47}^{3+}$ where the losses of individual fragments are clearly resolved and identified. The signal to noise ratio is typical of most of the experiments undertaken in this study. What should be recognised is that the mass and charge of the cluster and geometry of the mass spectrometer imposes a time window on what can be observed, and in this case that window lies between 10^{-5} and 10^{-4} s. In addition to those processes shown in Figure 2, it is highly likely that many alternative fragmentation pathways exist for $(C_6H_6)_{47}^{3+}$; however, fragments formed prior to

cluster ions entering the magnet or during their passage through the ESA may not reach the detector (see below for a comment on artefact peaks). The fragments shown in Figure 2 are representative of $(C_6H_6)_{47}^{3+}$ ions that have been extracted from the ion source, transmitted by the magnet and then undergone delayed unimolecular fragmentation in the second field-free region of the mass spectrometer.

III. THEORY

A. Electrostatic model

In two previous publications,[10,11] experimental and theoretical results have been presented from studies of Coulomb fission in doubly charged clusters. Results for the fission of $(NH_3)_n^{2+}$ clusters were successfully interpreted using a dielectric particle model due to Linse,[32] and subsequent results on $(H_2O)_n^{2+}$, $(NH_3)_n^{2+}$, $(CH_3CN)_n^{2+}$, $(C_5H_5N)_n^{2+}$ and $(C_6H_6)_n^{2+}$, were analyzed using a new analytical solution to describe the interaction between two charged dielectric particles due to Bichoutskaia *et al*.[30] This development in the theory of electrostatics has provided an accurate analytical solution to describe the electrostatic forces that exist between two dielectric particles.[30] The electrostatic force arising from the presence of permanent free charges, z_1 and z_2, residing on the surfaces of two interacting spherical particles is given as a generalization of Coulomb's law for point charges:[30]

$$\boldsymbol{F}_{12} = K \int dz_1(\boldsymbol{x_1}) \int dz_2(\boldsymbol{x_2}) \frac{\boldsymbol{x_1} - \boldsymbol{x_2}}{|\boldsymbol{x_1} - \boldsymbol{x_2}|^3}$$

$$= -\hat{\boldsymbol{z}} \frac{\partial}{\partial h} \left(K \int dz_1(\boldsymbol{x_1}) \int dz_2(\boldsymbol{x_2}) \frac{1}{|\boldsymbol{x_1} - \boldsymbol{x_2}|} \right) \Big|_{\sigma_{f,i}=const} \qquad (2)$$

where $\boldsymbol{x_1}$ and $\boldsymbol{x_2}$ are points on spheres 1 and 2, $\hat{\boldsymbol{z}}$ is a unit vector along the axis connecting the two spheres, h is their centre-to-centre separation and $K=1/4\pi\varepsilon_0 \approx 9\text{x}10^9$ VmC^{-1} is a constant

of proportionality, where ε_0 is the permittivity of free space (8.8542×10^{-12} Fm^{-1}). Each dielectric particle is assumed to be electrically neutral in its uncharged state with an equal number of positive and negative charges that are bounded by the surface of the particle, and the surface density of this bound charge is defined as $\sigma_{b,i}$. The total surface charge density, σ_i, is defined as the sum of free and bound charge densities: $\sigma_i = \sigma_{f,i} + \sigma_{b,i}$. The free charge on each particle is taken to be fixed, independent of the dielectric constant, and not to vary with separation between particles. It is also assumed that the density of free charge, $\sigma_{f,i}$, across the surface of a particle is uniform. In the absence of an external perturbation, such as an electric field, the bound surface charge on each particle is also assumed to be evenly distributed over the surface of a particle. Variations in electrostatic force acting on the system can arise as a result of polarisation of the bound surface charge density, $\sigma_{b,i}$, of one particle being induced by an electric field due to the presence of charge on a second particle. This redistribution of bound surface charge is represented by multipole terms that appear in an expression to describe the electrostatic force between particles.[30] No volume charges are taken into account as the overall effects of their polarisation in an external electric field cancel out. In order to derive an interaction energy from Equation (2), the analytical force has to be integrated numerically as a function of separation between the two charged spheres.

The solution to Equation (2) consists of two terms, a Coulomb term, which for like-charged spheres equates to repulsion, and an attractive term that arises from a mutual charge-induced polarisation of each of the spheres. The latter term is always attractive, is strongly dependent on the value of the dielectric constant, and at short separation, has the effect of moderating the magnitude of the Coulomb term. In earlier calculations on doubly charged clusters it was shown that the polarisation term can lower the Coulomb barrier, which in turn, can influence fragmentation pathways. Under certain circumstance, the magnitude of the polarisation term can lead to an attraction between particles carrying the same sign of charge.[33]

The theory is not designed to quantify the onset of Rayleigh instability in dielectric materials in terms of a liquid drop model; therefore no information is provide as to the magnitude of the barrier shown in figure 1 prior to fragmentation. Instead, the focus is on the interpretation of two pieces of experimental data that can be measured accurately and can be shown to reflect the physical properties of the fission products. Table 1 lists the bulk dielectric constants and densities of the molecular systems studied here; the latter numbers were used to calculate the radii of the cluster fragments.

B. Peak profile simulation

A key measurement in these experiments is the kinetic energy released (KER) as a consequence of Coulomb repulsion between the fragments as they separate. The earlier experiments on molecular dications showed the presence of a sequence of dish-shaped peak profiles,[10,11] from which it was possible to calculate a KER from the full width at half maximum (FWHM) for each peak assigned to a particular fission process.[31] However, this approach has limitations in that it relies heavily on the quality of the experimental data and is very sensitive to how accurately the width (ΔE) of a profile can be measured (KER is $\propto \Delta E^2$).[31] Thus, the poor signal-to-noise level seen on the edges of peaks that have been recorded at the upper end of the size and charge range, can lead to errors in KER values. In addition, peak broadening may originate from artefacts, which result from the fragmentation of precursor ions in the flight tube prior to their entering the magnet. A detailed summary of how artifact peaks arise through the fragmentation of cluster ions in various sections of the apparatus has been given in an earlier publication.[34] Taking just the width of a peak also attributes a single kinetic energy release to broadening,[31] and although the width may be dominated by a large value at or close to the Coulomb maximum shown in Figure 1, there will probably be a (narrow) spread of energy releases and these can contribute to the shape of a fragment ion's kinetic energy profile in the

laboratory-frame. For example, some partitioning of the Coulomb energy into internal modes of the fragments could add signal intensity to the central regions of a peak. In addition, the ions under discussion here are much heavier than the dications examined previously,[10,11] therefore, instrumental discrimination is less severe and so peak profiles that are markedly dish-shaped are less prevalent.

In order to improve the accuracy of energy release measurements, a method for calculating peak profiles proposed by Beynon and co-workers[35,36] has been adopted in the form of a Monte Carlo simulation. A random value for the kinetic energy release is selected from a rectangular distribution. From this energy a centre-of-mass velocity for the fragments is calculated on the assumption that, in the centre of mass frame, the scattering of ions is equally probable in all direction. This velocity is then transformed to the laboratory-frame as two components, v_z, which determines whether or not a fragment ion will pass through the final slit on the mass spectrometer, and v_{xy}, which determines how rapidly a fragment ion will reach the detector.[35,36] Since the position in the flight tube where fission occurs also influences the probability of an ion passing through the final slit, it is assumed that once a mass-selected ion has passed through the magnet, it has equal probability of fragmenting per unit time; therefore, the point of fragmentation in the flight tube is weighted by a random number selected from an exponential distribution. A total of 10^6 simulations were run for each set of conditions and for those ions calculated to have reached the detector, their centre-of-mass kinetic energies were transformed into a laboratory-frame peak profile. Matching the experimental data was an iterative process whereby the minimum and maximum of the rectangular energy distribution were adjusted until visual agreement was found. A summation of the kinetic energies of successful ion trajectories was used to calculate an average kinetic energy release, and it is this value that is compared with the theory. Table 2 shows results for $(C_6H_6)_{24}^{2+}$ where a comparison is made between taking the full width – half maximum of a peak to estimate the

energy release and the fitting procedure. As can be seen, the latter approach provides a more consistent set of results which then allow for an accurate comparison with the results from electrostatic theory. In relation to the work discussed here, figure 2 shows examples of peak profiles calculated for fragments resulting from the decay of $(C_6H_6)_{47}^{3+}$. Interestingly, the k=7 and k=8 peaks are calculated to have a shallow dish at the top and there is some evidence for that in the experimental data; however, as the mass of the detected ion increases, the dish disappears. The simulations also make it possible to identify processes where a peak profile is the product of multiple fragmentation steps. For example, where a single step at ~ U_{max} predicts a dish-shaped peak, but instead there is an intensity maximum at the centre (see below). It will also be shown that the simulations are able to distinguish between alternative fragmentation routes for +4 cluster ions.

IV RESULTS AND DISCUSSION

Reported here are the results of a series experiments where Coulomb fission in size-selected triply- and quadruply-charged clusters has been recorded. Three systems have been studied and these are: $(C_6H_6)_n^{z+}$, $(CH_3CN)_n^{z+}$ and $(C_4H_8O)_n^{z+}$, where the charge z is either 3 or 4. Table 3 lists the minimum stable size established for each molecular cluster as a function of charge z. Some of these numbers are lower that have previously been reported and this is as a consequence of observing fragmentation patterns rather than just appearance in a mass spectrum.[1] Also shown in Table 3 are estimates of the minimum stable size determined from the Rayleigh relationship. As can be seen, for the each of the dications and trications there is a reasonably close match between experiment and theory; however, there are quite large discrepancies for the +4 ions, with the Rayleigh expression consistently under-estimating the critical size by up to 25%. Measurements have been undertaken on clusters that are typically between 3 and 6 molecules above n_{cr}, which places the experiments within the X < 1 fission

regime, for which theory predict large fragments with low kinetic energies.[12] Previous experiments on dication clusters showed there to be a size range above n_{cr} over which clusters continued to exhibit Coulomb fission, and that is certainly the case for the examples studied here.

A. Triply charged cluster ions

Figure 3 shows a mass spectrum recorded following the electron impact ionization of neutral benzene clusters. The resolution of the mass spectrometer has been degraded significantly in order to enhance the appearance of triply charged clusters, $(C_6H_6)_n^{3+}$, and ions for *n* in the range 46-51 have been highlighted. Such a reduction in resolution does not have a marked influence on the kinetic energy measurements since the precursor ions maintain a laboratory-frame energy width of ~ 20 eV, which contrasts with a typical fission fragment energy width of ~ 200 eV. Figure 4 shows a fragmentation pattern recorded following the Coulomb fission of $(C_6H_6)_{49}^{3+}$ together with the results of simulating each of the peak profiles. The range of fragments observed is similar to that seen for $(C_6H_6)_{47}^{3+}$ in Figure 2. Table 4 summarises the experimental and calculated kinetic energy release data for three triply charged benzene clusters, where <*KER*> is the experimental average energy derived from a simulation of peak profiles and U_{max} is calculated from a solution to Equation (2). As can be seen, the agreement between experiment and theory is, for the most part, very good. It is interesting to note that the calculations predict a small decline in energy release as the fragment, k^+, increases in size, and this is supported to some extent by the experimental data. Further discussion of this aspect of the results will be presented below.

Figure 5 shows laboratory-frame kinetic energy profiles recorded for the fragments of $(CH_3CN)_{74}^{3+}$ together with the simulated results. The lighter mass of acetonitrile compared with benzene means that the fragment peaks are less well resolved and there is also some interference from other un-assigned fragmentation pathways. Overall, the agreement between

experiment and theory for the two examples shown in Table 5 is again good. The final triply charged system to be studied is that of tetrahydrofuran and figure 6 shows an example of experimental data together with the corresponding simulation results for the fragmentation of $(C_4H_8O)_{53}^{3+}$. The energy release data are summarised in Table 6, where it can be seen that the agreement between experiment and theory is not quite as good as that seen for the two previous examples. Across the three examples the results show a series of very asymmetric decay patterns to produce fragments that have high kinetic energies; two conclusions that do not fit with the predictions for multiply charged clusters where the fissility parameter, X, is < 1.[12]

B. Quadruply charged cluster ions

Clusters that carry four charges offer the possibility of two separate fragmentation routes, either the ions can decay into two smaller clusters, each carrying two charges, or fragmentation is asymmetric, with one large cluster carrying a charge of +3 accompanied by a smaller cluster with a charge of +1. Identifying and monitoring the fragmentation patterns of +4 ions proved to be difficult and there are features of the results that remain unexplained. In order to verify that for each example the mass spectrometer was tuned to a +4 ion one or both of two checks were undertaken. First, the loss of neutral molecules was recorded, and because this process is known to be accompanied by a very low kinetic energy release,[37] the corresponding peaks were easily resolved and assigned. Our previous study of +2 ions showed that ions close to the Coulomb limit can exhibit both neutral evaporation and Coulomb fission.[11] Second, ions selected for transmission through the magnet were often those that could easily be labelled. For example, $(C_6H_6)_{98}^{4+}$ has the same mass-to-charge ratio as $(C_6H_6)_{49}^{2+}$ but because fragments from the latter do not involve charge separation, they will not interfere with a decay pattern recorded above 7 keV for $(C_6H_6)_{98}^{4+}$. Figure 7 shows the results of a MIKE scan on the ion $(C_6H_6)_{98}^{4+}$ and where the laboratory-frame kinetic energies of the fragments

correspond to the ions $C_6H_6^+$, $(C_6H_6)_3^+$ and $(C_6H_6)_8^+$. Given the systematic nature of the fragmentation patterns observed for the +3 ions, the above pattern is unexpected and, as yet, unexplained. Again, it needs to be borne in mind that the mass spectrometer acts as a time filter, and so what are observed are processes that are most favourable on a time scale that is accessible during an experiment. A simulated peak profile is shown in figure 7 as a blue curve and kinetic energy release data derived from the profiles is given in Table 7. As can be seen, the agreement between theory and experiment for +3 and +1 fragments from both $(C_6H_6)_{98}^{4+}$ and $(C_6H_6)_{100}^{4+}$ is good; however, there is also the possibility for interpreting the fragmentation data in terms of two +2 fragments. That being the case, then the theory would predict a slightly higher release of kinetic energy; but more significant is the fact that if the energy release predicted for $(C_6H_6)_{98}^{4+}$ is fed back into the simulation program, then, as the red curve in figure 7 shows, the peak profile is predicted to be dish-shaped, which clearly does not match with the experimental result. The change in peak shape occurs because the fragment ion is now much lighter and has a slight increase in kinetic energy, and so is subject to more pronounced instrumental discrimination. Results from two further examples of +4 ion fragmentation, involving $(CH_3CN)_{165}^{4+}$ and $(C_4H_8O)_{110}^{4+}$, are shown in Table 7. For the former the agreement between experiment and theory is good, but as seen for the +3 ions, $(C_4H_8O)_{110}^{4+}$ exhibits a larger mis-match for the +3/+1 channel than is seen for the other multiply charged ions. Again for both examples there is the possibility that the positions of fragment ions could equate to decay pathways that form two +2 fragments; however, as has been shown for $(C_6H_6)_{98}^{4+}$, the magnitudes of the predicted energy releases from electrostatic theory are such that the resultant peaks would all emerge dish-shaped and such behaviour has not been observed in these experiments.

What is slightly surprising about the +4 results is the very small size of some of the fragment ions; however, the experiments by Mähr *et al.*[7] on the fragmentation of multiply

charged neon clusters showed a preference for dimer and trimer ions, and the imaging experiments of Hoener *et al*.[16] showed that monomer and dimer ions were also generated during the fission of neon dication clusters. Finally, the calculations of Miller *et al*.[38] on multiply charged clusters of Lennard-Jones particles show the ejection of individual charged particles from comparatively small clusters, but also provide evidence of a transition to more symmetric fission as the clusters increase in size.

C. Potential energy curves

Previous calculations on potential energy surfaces for dication molecular clusters,[10,11] showed that mutual charge-induced polarization of the fragments as they separated resulted in a lowering of the energy barrier to fragmentation. The effect was most pronounced in clusters composed of materials with high dielectric constants, i.e. water, but was also dependent on charge density. Therefore, the very asymmetric nature of the observed fragmentation patterns could be accounted for by having a small fragment with a high charge density accompanied by a much larger, more polarizable fragment. Taking $(H_2O)_{37}^{2+}$ as an example, the calculation showed that the barrier for loss of a singly charged cluster of 7 water molecules was slightly lower than that for the loss of 12. However, for clusters with low polarizabilities, for example, $(C_6H_6)_{24}^{2+}$, the reverse was calculated to be the case; the absence of any mutual polarization meant that the electrostatic barrier was strongly influenced by Coulomb repulsion

In order to explore how fragment energy surfaces evolve as a function of increased charge on the precursor cluster, a series of potential energy curves have been calculated for several of the fragment ion combinations discussed above. Figure 8 shows the results for benzene clusters where curves for the dication are reproduced together with results calculated for fragments emerging from the +3 and +4 ions. Similar to the dication, the ordering of the energy curves for triply charged ions is determined solely by electrostatic repulsion and

therefore the high charge density on the smaller fragments leads to an increase in the electrostatic barrier. The consequences can be seen in table 4 where the predicted kinetic energy release drops in magnitude as the fragment size (k) increases and a similar result can be seen in table 5 for the +4 ions, and for both charge states the experimental data provide good evidence to support this effect. Figure 9 shows potential energy curves calculated for acetonitrile clusters. The effects of an increase in polarizability are evident from the decline in Coulomb repulsion seen at short separation. For the dication this results in a reversal of the ordering of kinetic energy releases from that seen for benzene clusters. However, for the +3 and +4 cluster ions, the higher charge density present on the smaller of the fragments appears to have greater influence on the repulsive rather than the attractive contribution to the electrostatic barrier. There is again some experimental evidence in table 5 to support this conclusion; however, the drop in both the experimental and predicted kinetic energy release as a function of k is not as pronounced as that seen for the benzene clusters. The very high charge density present on CH_3CN^+ clearly has a very noticeable effect on the ion's interaction with the complementary product $(CH_3CN)_{164}^{3+}$ at short separation; but as with the other high charge cations, the longer range Coulomb repulsion ultimately determines the magnitude of the electrostatic barrier and hence the kinetic energy release.

Figure 10 compares the potential energy curve calculated for one of the very small fragment ions observed from $(CH_3CN)_{165}^{4+}$ with curves corresponding to some alternative, more symmetric fragmentation pathways, which could be taking place in the mass spectrometer. The charge symmetric route leading to $(CH_3CN)_{98}^{2+}$ and $(CH_3CN)_{67}^{2+}$ has already been eliminated on the grounds of predicted peak shape (see figure 7); however, it can also be seen that this pathway has a higher electrostatic barrier than is calculated for those pathways that are detected. Also shown are calculated electrostatic barriers for +3/+1 pathways that are increasingly more symmetric in terms of the numbers of molecules contained in each fragment.

As can be seen, greater symmetry is accompanied by a significant decrease in the height of the barrier. At short separation the slight change in curvature seen on the -40^+ curve and more so on the -60^+ curve is due to increased charge density on the +3 ion interacting with a singly charged cluster that is gradually becoming more polarizable. The question then is why these fragmentation pathways are not observed in the experiments? There are two more obvious possibilities: (i) they are taking place, but on a very much shorter timescale than can be observed in a MIKE scan; (ii) the electrostatic contribution is just one component of the energy barrier that a multiply charged cluster has to overcome in order to fragment. In figure 1, the quantity $E_{barrier}$ has to be surmounted before the two fragments can begin to separate and it is not known how the magnitude of this energy will vary for fragments ranging in size from 5 to 60 molecules. However, if the precursor cluster ion is densely packed, then it can probably be assumed that the more molecules contained in a fragment, the greater the number of intermolecular bonds that are required to break during fragmentation. Hence, $E_{barrier}$ should increase with the size of the fragment.

There are clearly a number of issues which can influence the fragmentation patterns observed for multiply charged clusters on the timescales discussed here. For the case of dications composed of polar materials, it has been concluded that size asymmetry is driven by small differences in the electrostatic barrier experienced by the fragments as they begin to separate. However, for non-polar dications and all of the +3 and +4 ions studied, that does not appear to be the case and the calculations would imply that far less asymmetry should be present in the fragmentation patterns. The fact that those fragments that are recorded are also subject to a constraint imposed by a finite time window suggests that it is the latter that has an over-riding influence on the outcome of these experiments.

V CONCLUSION

For three separate triply and quadruply charged molecular clusters, $(C_6H_6)_n^{z+}$, $(CH_3CN)_n^{z+}$ and $(C_4H_8O)_n^{z+}$, where z is either 3 or 4 and n is close to the charge instability limit, experimental measurements on their fragmentation patterns have provided evidence of charge separation and a significant asymmetry in the sizes of the two product ions. Through the simulation of fragment ion peak profiles it has been possible to extract accurate kinetic energy release values associated with Coulomb repulsion between the charged species as they separate. Complementary calculations using theory developed to study interactions between charged particles composed of dielectric materials[30] have provided a quantitative account of the kinetic energy measurements in terms of a combination of attractive, polarization interactions and Coulomb repulsion between like-charged fragment spheres. The match between experiment and theory for benzene and acetonitrile clusters is excellent, which in terms of the theory, is very encouraging because the two materials have quite dissimilar properties with regard to polarizability. The less good agreement for tetrahydrofuran clusters is, at first sight, disappointing; however, even for the worst case the mismatch between experiment and theory for THF is only 10%.

For charged particles or clusters, such as those studied here, where the fissility parameter, X is < 1, fission is predicted to involve a few large fragments which should emerge with low kinetic energies.[12] Although the observed fragmentation patterns are very asymmetric, the occurrence of fragments larger than those seen in the experiments cannot be ruled out; however, the close match between electrostatic theory and the experimental results would suggest that none of the fragments will have low kinetic energies. Both experiment and theory confirm that the magnitude of the electrostatic interaction between the two charged species as they separate does not scale as the product z_1z_2, which would be the case for point charges.

Instead, the results support the assumption that charge is uniformly distributed across the surface of each sphere.

Acknowledgements

AJS and CH would like to thank Nottingham University for financial support for the programme of experiments and for the award of a postgraduate studentship to CH. E.B. acknowledges financial support through an ERC Starting Grant, an EPSRC Career Acceleration Fellowship and a New Directions for EPSRC Research Leaders Award (EP/G005060). EBL is supported by a PhD scholarship from the Brazilian Government's Science Without Borders programme (CAPES: 0702/13-7). AJS would like to thank Prof. Gareth Brenton for bringing techniques for simulating peak profiles to his attention.

[1] O. Echt, D. Kreisle, E. Recknagel, J. J. Saenz, R. Casero, and J. M. Soler, Phys. Rev. A **38**, 3236 (1988).

[2] A. J. Stace, Phys. Rev. Lett. **61**, 306 (1988).

[3] A. J. Stace, Chem. Phys. Lett. **174**, 103 (1990).

[4] N. G. Gotts and A. J. Stace, Phys. Rev. Lett. **66**, 21 (1991).

[5] N. G. Gotts and A. J. Stace, J. Chem. Phys. **95**, 6175 (1991).

[6] N. G. Gotts, P. G. Lethbridge and A. J. Stace, J. Chem. Phys. **96**, 408 (1992).

[7] I. Mähr, F. Zappa, S. Denifl, D. Kubala, O. Echt, T. D. Märk and P. Scheier, Phys. Rev. Lett. **98**, 023401-1 (2007).

[8] D. Kreisle, K. Leiter, O. Echt and T. D. Märk, Z. Phys. D: At. Mol. Clusters, **3**, 319 (1986).

[9] C. Bréchignac, Ph. Cahuzac, N. Kébaïli and J. Leygnier, Phys. Rev. Lett. **81**, 4612 (1998).

[10] Wu, G.; Chen, X.; Stace, A. J.; Linse, P. J. Chem. Phys. **134**, 031103 (2011).

[11] X. Chen, E. Bichoutskaia and A. J. Stace, J. Phys. Chem. A **117**, 3877 (2013).

[12] I. Last, Y. Levy and J. Jortner, J. Chem. Phys. **123**, 154301 (2005).

[13] C. Bréchignac, Ph. Cahuzac, M. de Frutos, P. Garnier and N. Kebaili, Phys. Rev. B **53**, 1091 (1996**)**.

[14] J. G. Gay and B. J. Berne, Phys. Rev. Lett. **49**, 194 (1982).

[15] Lord Rayleigh, Philos. Mag. A **14**, 184 (1882).

[16] M. Hoener, C. Bostedt, S. Schorb, H. Thomas, L. Foucar, O. Jagutzki, H. Schmidt-Böcking, R. Dörner and T. Möller, Phys. Rev. A **78**, 021201 (2008).

[17] P. Kebarle and U. H. Verkerk, Mass Spectrom. Rev. **28**, 898 (2009).

[18] S. Crotti, R. Seraglia and P. Traldi, Eur. J. Mass Spectrom. **17**, 85 (2011).

[19] R. L. Grimm and J. L. Beauchamp, Anal. Chem. **74**, 6291 (2002).

[20] J. N. Smith, R. C. Flagan and J. L. Beauchamp, J. Phys. Chem. A, **106**, 9957 (2002).

[21] P. Kebarle and M. Pescke, Anal. Chem. Acta, **406**, 11 (2000).

[22] C. J. Hogan, Jr., P. Biswas and D. Chen, J. Phys. Chem. **113**, 970 (2009).

[23] I. G. Loscertales and F. de la Mora, F. J. Chem. Phys. **103**, 5041 (1995).

[24] M. Gamero-Castano and F. de la Mora, F. J. Mass Spectrom. **35**, 790 (2000**)**.

[25] M. Gamero-Castano and F. de la Mora, F. J. Chem. Phys. **113**, 815 (2000).

[26] M. Dole, L. L. Mack, R. L. Hines, R. C. Mobley, L. D. Ferguson, and M. B. Alice, J. Chem. Phys. **49**, 2240 (1968).

[27] B. A. Winger, K. J. Light-Wahl, R. R. Ogorzalek Loo, H. R. Udseth, and R. D. Smith, J. Am. Soc. Mass Spectrom. **4**, 536 (1993).

[28] J. V. Iribarne, and B. A. Thomson, J. Chem. Phys. **64**, 2287 (1976).

[29] B. A. Thomson, and J. V. Iribarne, J. Phys. Chem. **71**, 4451 (1979).

[30] E. Bichoutskaia, A. L. Boatwright, A. Khachatourian and A. J. Stace, J. Chem. Phys. **133**, 024105 (2010).

[31] R. G. Cooks, J. H. Beynon, R. M. Caprioli and G. R. Lester, *Metastable Ions*, (Elsevier: Amsterdam, 1973).

[32] P. Linse J. Chem. Phys. **128**, 21405 (2008).

[33] A. J. Stace, A. L. Boatwright, A. Khachatourian and E. Bichoutskaia, J. Colloid Interface Sci. **354**, 417 (2011).

[34] P. Lethbridge and A. J. Stace, J. Chem. Phys. **89**, 4062 (1988).

[35] J. E. Szulekjo, A. M. Amaya, R. P. Morgan, A. G. Brenton and J. H. Beynon, Proc. R. Soc. Lond. A **373**, 1 (1980).

[36] A. M. Amaya, A. G. Brenton, J. E. Szulekjo and J. H. Beynon, Proc. R. Soc. Lond. A **373**, 13 (1980).

[37] C. A. Woodward and A. J. Stace, J. Chem. Phys. **94**, 4234 (1991).

[38] M. A. Miller, D. A. Bonhommeau, C. P. Moerland, S. J. Gray and M-P. Gaigeot, Mol. Phys. **113**, 2428 (2015).

Figure captions.

Figure 1. A potential energy curve for the coulomb fission of the multiply charged cluster $(M)_n^{z+}$ into fragments $(A)_{n-k}^{z-x+}$ and $(B)_k^{x}$. That feature of the electrostatic potential energy surface which is responsible for promoting the release of kinetic energy is denoted as U_{max}.

Figure 2. Coulomb fission fragmentation pattern recorded for the triply charged benzene cluster $(C_6H_6)_{47}^{3+}$ using the MIKE technique. The intensities of the product +2 ions have been recorded as a function of laboratory-frame kinetic energy and the values of the complementary

single charged fragments are given above each peak. Shown as blue lines are peak profiles simulated using techniques outlined in the text.

Figure 3. Example of a mass spectrum recorded in a region where triply charged benzene clusters, $(C_6H_6)_n^{3+}$, are present. Clusters with specific values of *n* are highlighted.

Figure 4. As for Figure 2, but for the triply charged benzene cluster $(C_6H_6)_{49}^{3+}$.

Figure 5. As for Figure 2, but for the triply charged acetonitrile cluster $(CH_3CN)_{74}^{3+}$.

Figure 6. As for Figure 2, but for the triply charge tetrahydrofuran cluster $(C_4H_8O)_{53}^{3+}$.

Figure 7. Coulomb fission fragmentation pattern recorded for the quadruply charged benzene cluster $(C_6H_6)_{98}^{4+}$ using the MIKE technique. The intensities of the product +3 ions have been recorded as a function of laboratory-frame kinetic energy and the values of the complementary single charged fragments are given above each peak. Shown as a blue line is a peak profile simulated on the assumption that the fragments carry charges of +3 and +1. Shown as a red line is a simulation where it has been assumed that the fragments are two +2 ions.

Figure 8. Electrostatic potential energy curves calculated to represent the Coulomb barrier experienced by two fission fragments from a multiply-charged benzene cluster as they

separate. The curves have been calculated for each of the ions shown on the assumption that it has lost a singly charged cluster containing the number of molecules shown against each curve.

Figure 9. As for Figure 9, but for multiply-charged acetonitrile clusters.

Figure 10. Electrostatic potential energy curves calculated to represent the Coulomb barrier experienced by two fission fragments from $(CH_3CN)_{165}^{4+}$. The lower curves are representative of +3/+1 pathways and the upper curve illustrates the consequences of having a pathway leading to the appearance of two +2 ions.

Table 1. Bulk molecular properties used to provide input for the calculation of electrostatic interactions between fragment ions following the Coulomb fission of multiply charged clusters.

Molecule	Dielectric constant (ε_r)	Density / kg m^3
C_6H_6	2.3	875.6
CH_3CN	39	786
C_4H_8O	7.5	889

Table 2. Sample data on the fragmentation of $(C_6H_6)_{24}^{2+}$ that is used to illustrate the advantage of simulating peak profiles to extract accurate values for the release of kinetic energy following Coulomb fission.

Precursor	Fragment (k^+)	*KER* / eV #	<*KER*>/eV !	U_{max} / eV
$(C_6H_6)_{24}^{2+}$	7	*	0.86	0.92
	8	0.91	0.86	0.92
	9	0.98	0.86	0.92
	10	0.92	0.86	0.91
	11	0.42	0.86	0.91

Single energy release calculated from the FWHM.
* Accurate measurement not possible.
! Calculated from a simulation of the peak profile.

Table 3. The minimum stable size (n_{crit}) observed for each molecular cluster carrying a charge of z. Also presented are critical sizes calculated from the Rayleigh relationship given in the text.

Cluster and charge state (z)	Experimental $n_{cr}(z)$	Calculated $n_{cr}(z)$
$(C_6H_6)_n^{z+}$		
2+	17	20
3+	43	43
4+	96	77
$(CH_3CN)_n^{z+}$		
2+	28	30
3+	66	69
4+	161	122
$(C_4H_8O)_n^{z+}$		
2+	24	22
3+	51	48
4+	107	86

Table 4. Experimental fragmentation pathways recorded following the mass-selection of a series of triply charged benzene clusters. The size of the fragment ion loss from each cluster is given by k^+, the kinetic energy released as a consequence of Coulomb repulsion between the separating fragments is given by <*KER*>, and the calculated height of the electrostatic barrier is given by U_{max}.

Precursor cluster	Fragment (k^+)	<*KER*> / eV	U_{max} / eV
$(C_6H_6)_{47}^{3+}$	4	1.57	1.62
	5	1.57	1.60
	6	1.56	1.58
	7	1.56	1.56
	8	1.56	1.55
$(C_6H_6)_{48}^{3+}$	5	1.56	1.59
	6	1.56	1.57
	7	1.56	1.56
	8	1.56	1.54
	9	1.56	1.53
$(C_6H_6)_{49}^{3+}$	5	1.57	1.58
	6	1.57	1.56
	7	1.55	1.55
	8	1.53	1.53

Table 5. As for Table 4, but for triply charged acetonitrile clusters.

Precursor cluster	Fragment (k^+)	$< KER >$ eV	U_{max} / eV
$(CH_3CN)_{69}^{3+}$	5	1.53	1.53
	6	1.53	1.53
	7	1.53	1.53
	8	1.52	1.53
	9	1.52	1.53
	10	1.52	1.52
$(CH_3CN)_{74}^{3+}$	5	1.43	1.49
	6	1.43	1.49
	7	1.43	1.49
	8	1.42	1.49
	9	1.42	1.49
	10	1.42	1.49

Table 6. As for Table 4, but for a triply charged tetrahydrofuran cluster.

Precursor cluster	Fragment (k^+)	<*KER*> / eV	U_{max} / eV
$(C_4H_8O)_{53}^{3+}$	8	1.46	1.48
	9	1.55	1.47
	10	1.55	1.46
	11	1.55	1.45
	12	1.54	1.44

Table 7. Experimental fragmentation pathways recorded following the mass-selection of a series of quadruply charged molecular clusters. The size of a fragment ion from each cluster is given by either k^+ for the case of a +3/+1 pathway or k^{2+} for the case of two +2 fragments. The kinetic energy released as a consequence of Coulomb repulsion between the separating fragments is given by <*KER*>, and the calculated height of the electrostatic barrier is given by U_{max}.

Precursor cluster	Fragment (k^+)	<*KER*> / eV	U_{max} / eV
$(C_6H_6)_{98}^{4+}$	1	2.00	2.12
	3	2.00	2.01
	8	1.98	1.94
$(C_6H_6)_{100}^{4+}$	2	2.00	2.07
	5	1.99	1.99
	9	1.98	1.91
$(CH_3CN)_{165}^{4+}$	1	-	1.83
	3	1.90	1.83
	5	1.90	1.82
$(C_4H_8O)_{110}^{4+}$	10	1.66	1.83
	12	1.66	1.81
	14	1.65	1.78
	Fragment (k^{2+})		
$(C_6H_6)_{98}^{4+}$	35	2.18	2.30
$(CH_3CN)_{165}^{4+}$	67	1.96	2.10
$(C_4H_8O)_{110}^{4+}$	45	2.17	2.17

Figure 1.

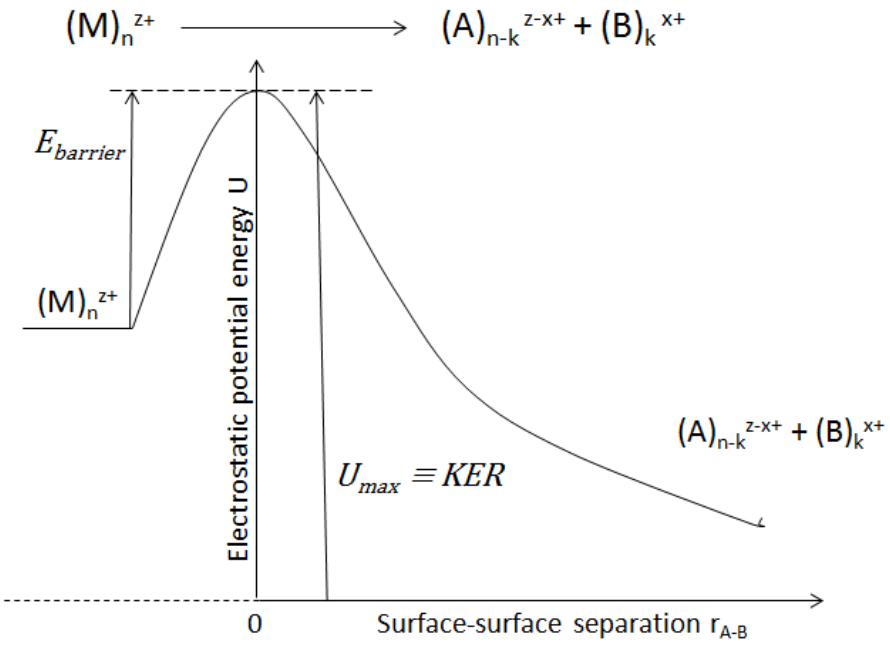
$(M)_n^{z+}$
$(A)_{n-k}^{z-x+} + (B)_k^{x+}$
$E_{barrier}$
$(M)_n^{z+}$
Electrostatic potential energy U
$U_{max} \equiv KER$
$(A)_{n-k}^{z-x+} + (B)_k^{x+}$
0
Surface-surface separation r_{A-B}

Figure 2

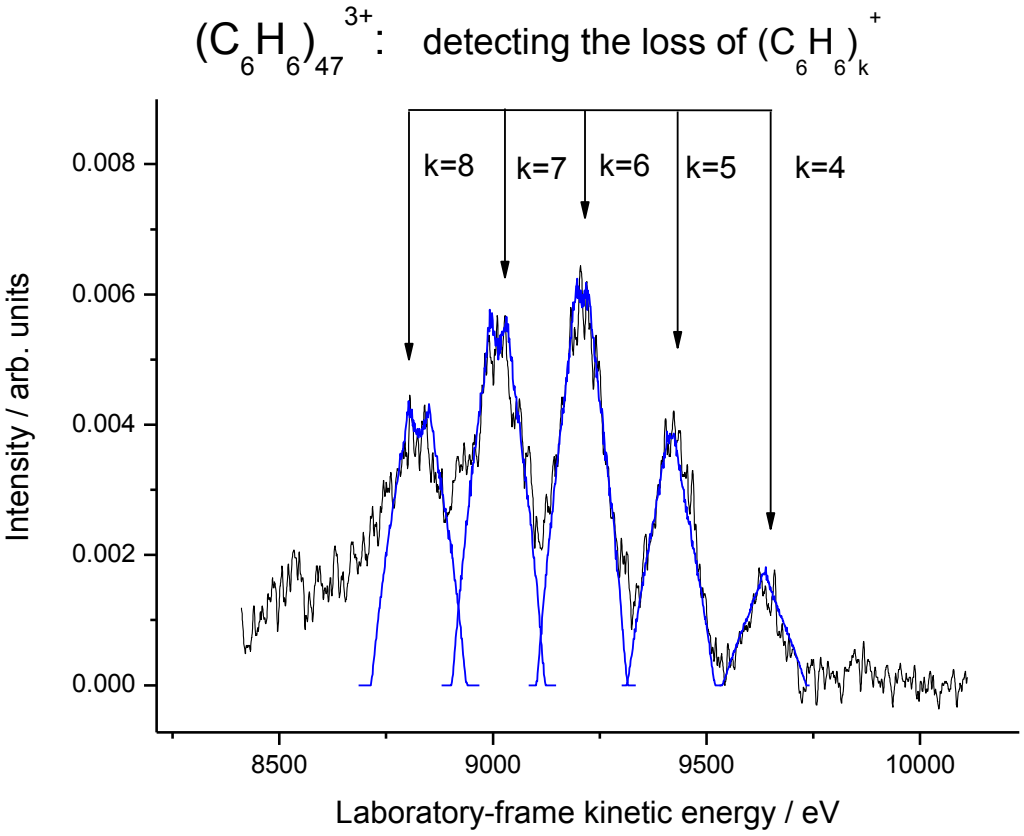
(C6H6)47 3+: detecting the loss of (C6H6)k +
k=8
k=7
k=6
k=5
k=4
Intensity / arb. units
0.000
0.002
0.004
0.006
0.008
8500
9000
9500
10000
Laboratory-frame kinetic energy / eV

Figure 3.

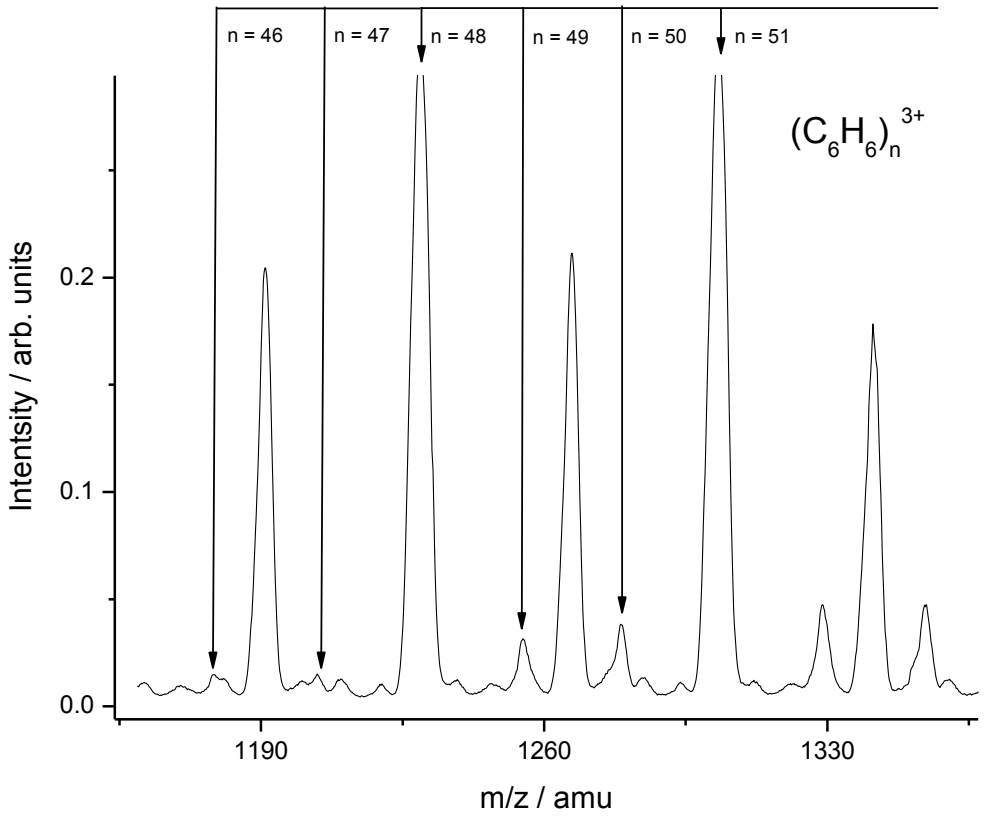
n = 46
n = 47
n = 48
n = 49
n = 50
n = 51
$(C_6H_6)_n^{3+}$
Intentsity / arb. units
0.0
0.1
0.2
1190
1260
1330
m/z / amu

Figure 4

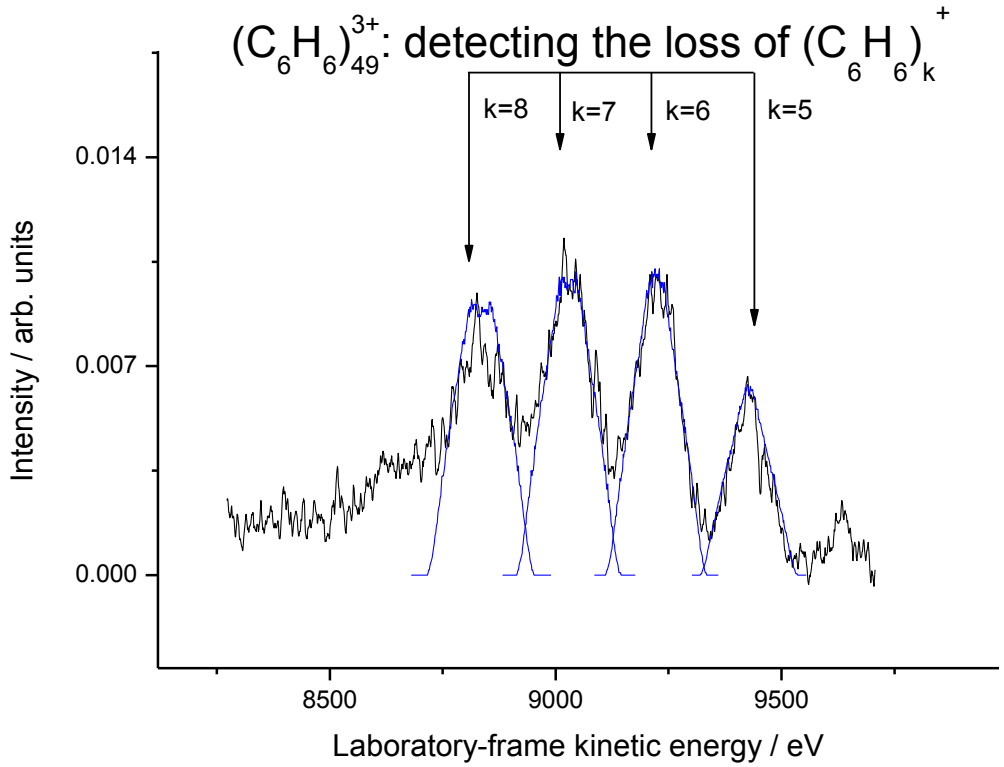
$(C_6H_6)_{49}^{3+}$: detecting the loss of $(C_6H_6)_k^+$
k=8
k=7
k=6
k=5
0.014
0.007
0.000
Intensity / arb. units
8500
9000
9500
Laboratory-frame kinetic energy / eV

Figure 5.

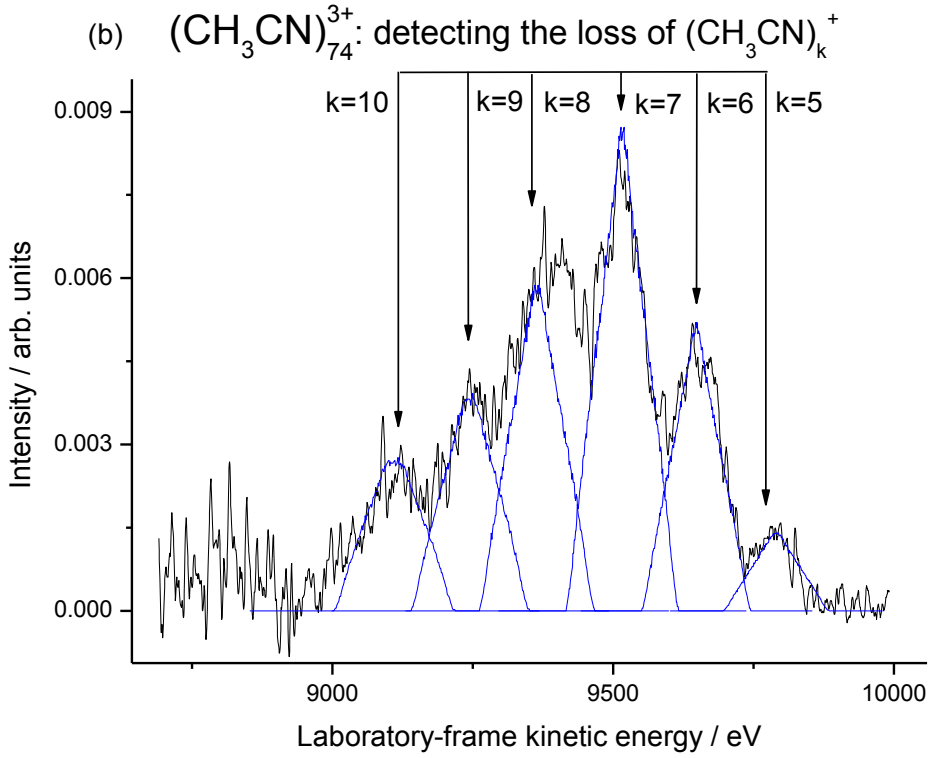
(b) $(CH_3CN)_{74}^{3+}$: detecting the loss of $(CH_3CN)_k^+$
k=10
k=9
k=8
k=7
k=6
k=5
0.009
0.006
0.003
0.000
Intensity / arb. units
9000
9500
10000
Laboratory-frame kinetic energy / eV

Figure 6.

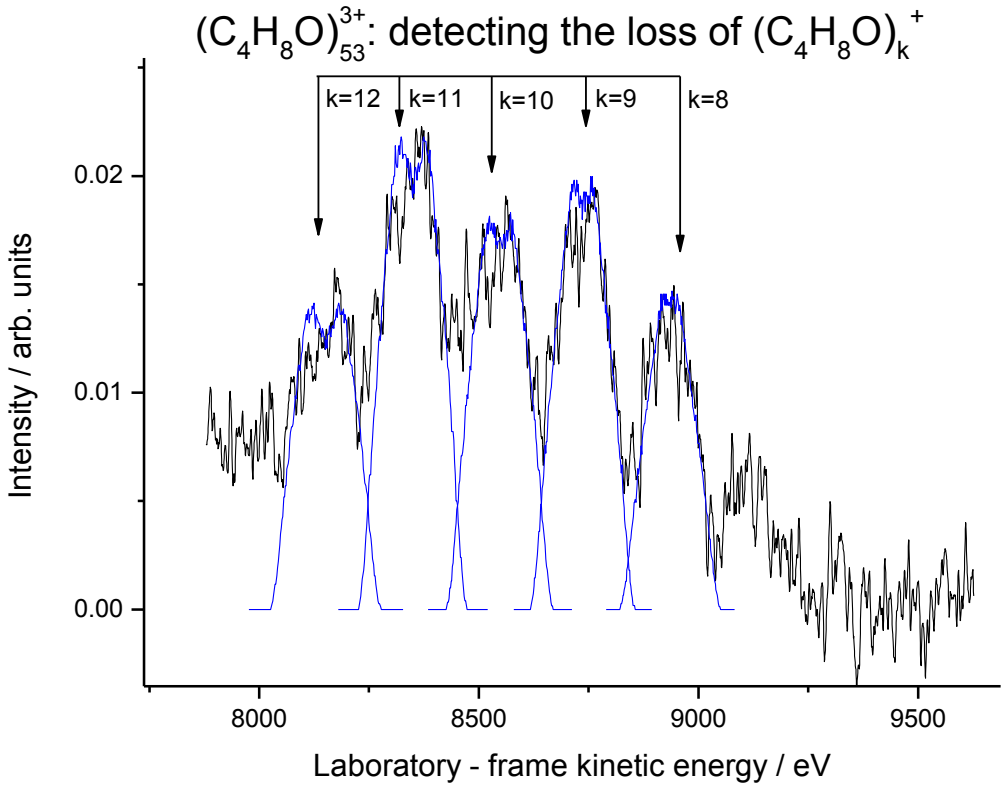

Figure 7.

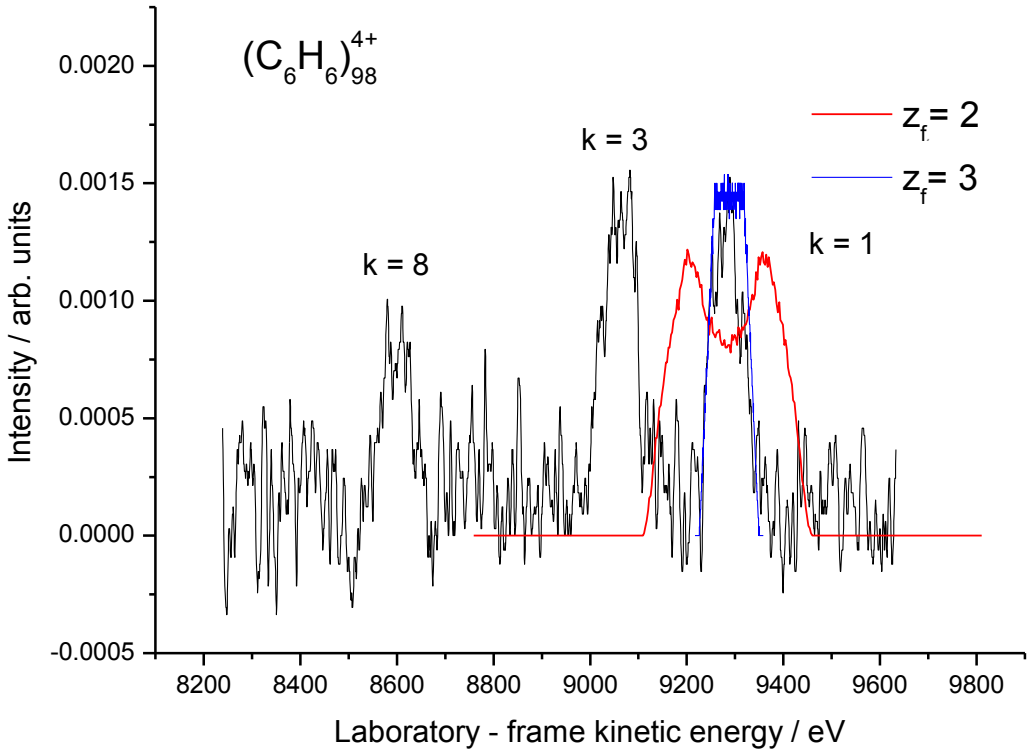
$(C_6H_6)_{98}^{4+}$
z_f= 2
z_f= 3
k = 3
k = 8
k = 1
Intensity / arb. units
0.0020
0.0015
0.0010
0.0005
0.0000
-0.0005
8200
8400
8600
8800
9000
9200
9400
9600
9800
Laboratory - frame kinetic energy / eV

Figure 8.

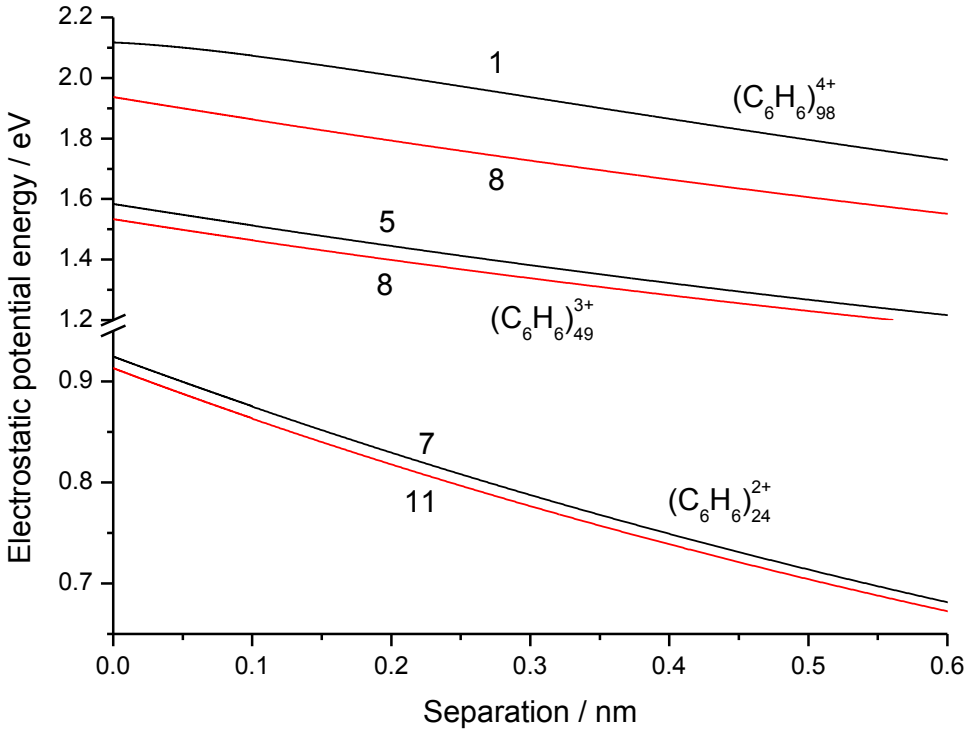
Electrostatic potential energy / eV
Separation / nm
2.2
2.0
1.8
1.6
1.4
1.2
0.9
0.8
0.7
0.0
0.1
0.2
0.3
0.4
0.5
0.6
1
8
5
8
7
11
$(C_6H_6)_{98}^{4+}$
$(C_6H_6)_{49}^{3+}$
$(C_6H_6)_{24}^{2+}$

Figure 9

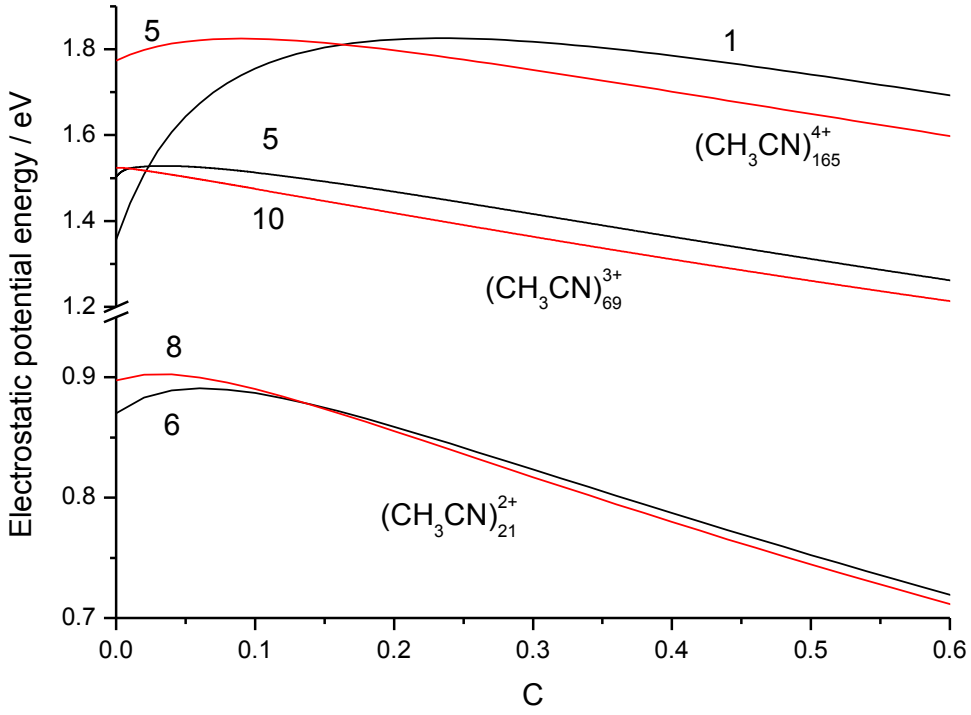
Electrostatic potential energy / eV
C
5
1
5
10
8
6
$(CH_3CN)^{4+}_{165}$
$(CH_3CN)^{3+}_{69}$
$(CH_3CN)^{2+}_{21}$
1.8
1.6
1.4
1.2
0.9
0.8
0.7
0.0
0.1
0.2
0.3
0.4
0.5
0.6

Figure 10.

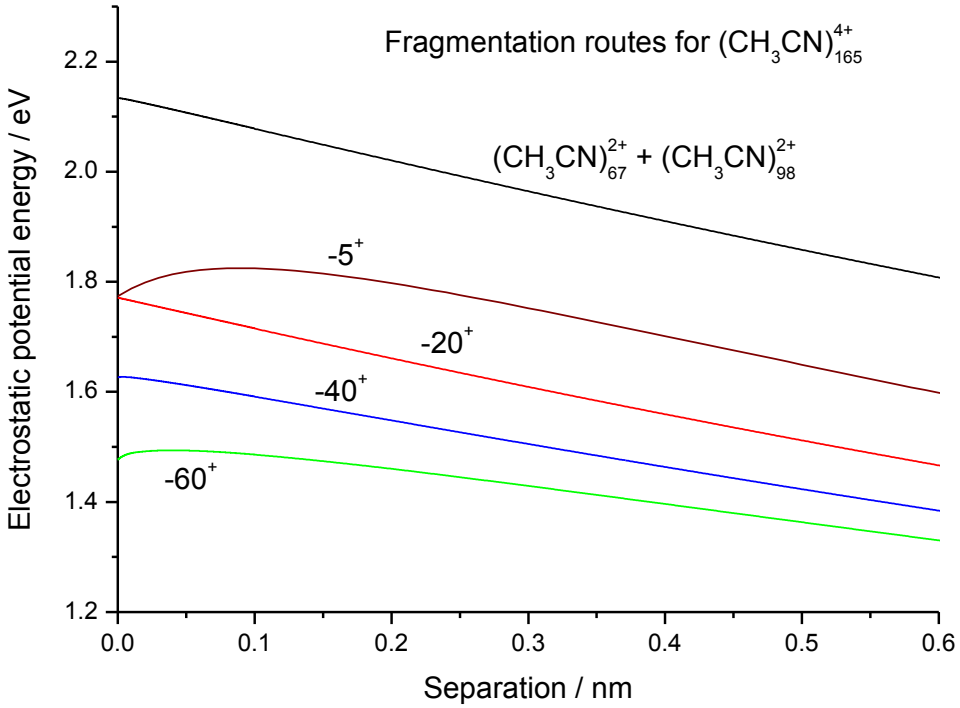
Fragmentation routes for $(CH_3CN)^{4+}_{165}$
$(CH_3CN)^{2+}_{67}$ + $(CH_3CN)^{2+}_{98}$
-5^+
-20^+
-40^+
-60^+
Electrostatic potential energy / eV
Separation / nm
2.2
2.0
1.8
1.6
1.4
1.2
0.0
0.1
0.2
0.3
0.4
0.5
0.6